Miner Deposita (2007) 42:613–626
DOI 10.1007/s00126-007-0127-5

ARTICLE

The origin of the Tongkeng-Changpo tin deposit, Dachang metal district, Guangxi, China: clues from fluid inclusions and He isotope systematics

Cai Minghai · Mao Jingwen · Liang Ting · Franco Pirajno · Huang Huilan

Received: 11 November 2005 / Accepted: 25 January 2007 / Published online: 17 February 2007

Abstract Tongkeng-Changpo is the largest tin deposit within the giant Dachang polymetallic tin ore field in Guangxi, southern China, which is part of a large skarn system associated with Cretaceous granitoids. The Tongkeng-Changpo mineralization consists of veins and stockworks in the upper levels and replacement stratiform orebodies (mantos) at lower levels. Based on textural relationships, three major mineralizing stages can be recognized: stage I with cassiterite, sulphides, stannite, tourmaline, and quartz; stage II with cassiterite, sulphides, sulphosalts, quartz, and calcite; and stage III with calcite as the main phase. The study of fluid inclusions has shown that there are two main fluid types: CO_2 and NaCl-H_2O. Homogenization temperatures are 270 to 365°C, 210 to 240°C, and 140 to 190°C for stages I, II, and III, respectively. Salinities range from 1 to 7 wt.% NaCl equiv. in the early ore stage and 3 to 10 wt.% NaCl equiv. in the late stages. Laser Raman Spectroscopy indicates that the inclusion fluids in stages I and II were of carbono-aqueous composition, with minor amounts of CH_4 and H_2S, whereas those in stage III were aqueous. Helium isotopic analyses of inclusion fluids indicate that the $^3He/^4He$ ratios in the ore veins are in between 1.2 to 2.9 Ra ($Ra=1.4\times10^{-6}$, modern atmospheric ratio), and range from 1.6 to 2.5 Ra in the stratiform orebodies. This range of $^3He/^4He$ ratios is significantly higher than that of crustal fluids (0.01–0.05 Ra). The similar characteristics of fluid inclusions and their He isotopic composition, as well as age constraints, indicate that the ore veins and stratiform orebodies of the Tongkeng-Changpo deposit formed from the same hydrothermal system, likely related to granite intrusions of the Mesozoic Yanshanian tectono-thermal event. In addition, the high R/Ra ratios indicate a mantle contribution in the ore fluids.

Keywords Tin · Mineralization fluid · Inclusions · He · Isotopes · Tongkeng-Changpo · Polymetallic tin · Dachang · Guangxi · China

Editorial handling: G. Beaudoin

C. Minghai (✉)
Faculty of Resource and Environment, Guangxi University,
Daxue Road 100, Nanning,
530004 Guangxi, China
e-mail: gxdxcmh@163.com

M. Jingwen
Institute of Mineral Resources,
Chinese Academy of Geological Sciences,
26 Baiwanzhuang Road,
Beijing 100037, China
e-mail: jingwenmao@263.net

L. Ting
Department of Geology and Mineral Resources,
Chang'an University,
Cuihua Road, Xi'an,
710054 Shaanxi, China

F. Pirajno
Geological Survey of Western Australia,
100 Plain Street,
East Perth WA 6004, Australia

H. Huilan
Yichang Institute of Geology and Mineral Resources,
China Geological Survey,
Guangyao Road 37, Yichang,
443003 Hubei, China

Introduction

The Dachang polymetallic tin ore field is one of the largest in the world. It is located in Nandan County, Guangxi

Zhuang Autonomous Region (or Guangxi province), South China. The ore field is situated in the Yangtze platform, near the northern margin of the South China Fold Belt (or Cathaysia), and contains resources of approximately 110 MT at 1% Sn metal, 3 to 5% other metals (Zn, In, Sb, Cu), and 100 to 300 ppm Ag. The economic deposits in the ore field (Figs. 1 and 2) include the Tongkeng-Changpo, Bali, and Longtoushan polymetallic Sn deposits (western ore belt), the Lamo Cu–Zn skarn deposit and the Chashan Sb deposit (central ore belt), and the Dafulou, Huile, and Kangma polymetallic Sn deposits (eastern ore belt). The Tongkeng-Changpo tin deposit accounts for about 60% of the tin resource in the Dachang ore field with an in situ reserve of 650,000 T of tin metal. It is the largest tin producer in China, yielding 25,000 T of tin metal/year.

The Dachang ore field is essentially a large skarn system, which is associated with a Cretaceous granitic pluton (Longxianggai Granite). The skarn system, which is zoned from the granite contacts both laterally and vertically,

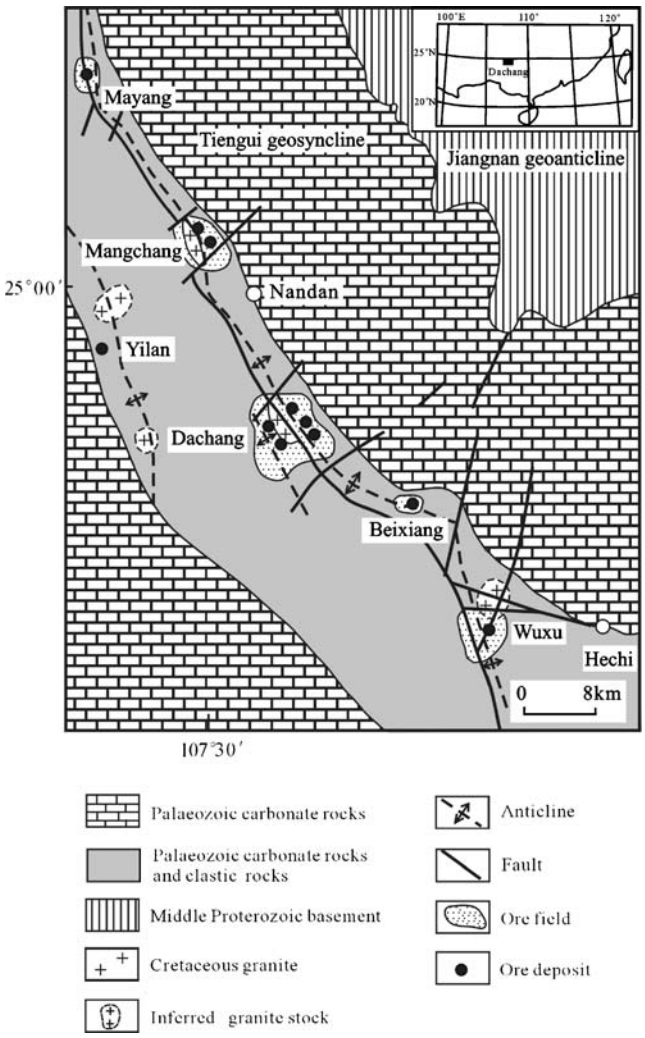

Fig. 1 Simplified map of the Nandan-Hechi fold-and-thrust belt (from Han et al. 1997)

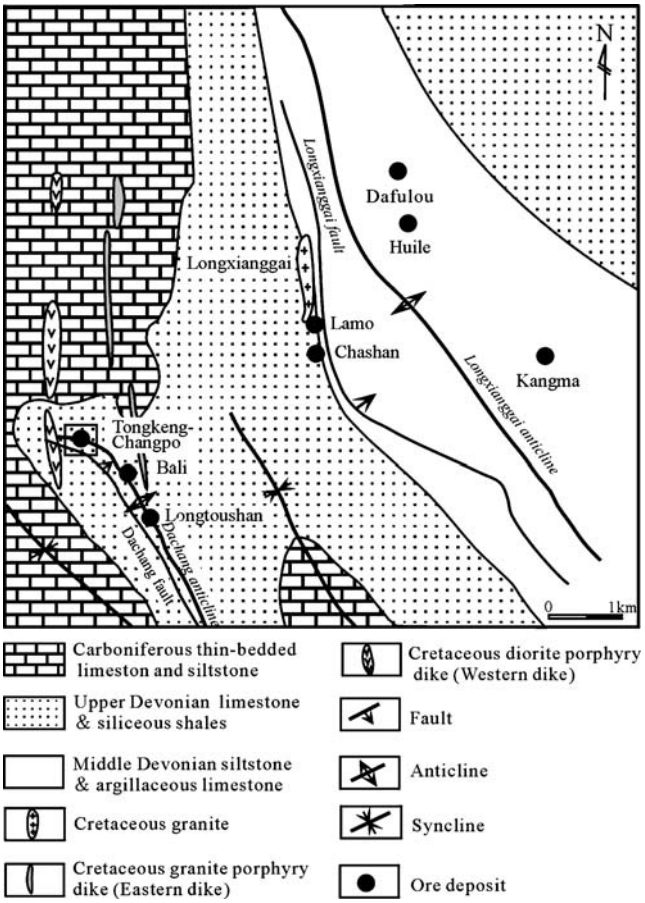

Fig. 2 Geologic map of the Dachang ore field (modified from Tongkeng-Changpo mine maps)

is in the Devonian carbonate rocks (Fu et al. 1993). Details of the distal and proximal skarn silicates, sulphides, and oxides can be found in Lattanzi et al. (1989) and Fu et al. (1991, 1993). In the Tongkeng-Changpo deposit, this zonation is especially well developed vertically, with Sn–Zn dominant in stratiform carbonate and replacement distal skarns at depth, to the veins and stockworks with Sn dominant closer to the surface.

In the past several decades, numerous Chinese and foreign researchers have studied the Dachang tin field, with most of the studies focusing on the genesis of the ore deposits. All of these researchers agreed that the Tongkeng-Changpo ore veins and stockworks are related to the Longxianggai Granite, within the central Dachang ore field (Fig. 2; Tanelli and Lattanzi 1985; Lei 1986; Lattanzi et al. 1989; Fu et al. 1991, 1993; Chen et al. 1993; Han et al. 1997; Ye et al. 1999; Qin et al. 2002). However, the genesis of the stratiform orebodies in the lower parts of the ore zone is still debated. Most researchers suggested that stratiform ores were formed by the replacement of Devonian carbonate rocks and shales induced by hydrothermal fluids originating from the Cretaceous Longxianggai Granite, resulting in a typical carbonate skarn and replacement

sulphide deposit (Chen et al. 1993; Fu et al. 1991, 1993; Ye et al. 1999; Wang et al. 2004). However, others have proposed that the stratiform ores were the result of submarine exhalations during the Devonian (Cai and Zhang 1983; Lei 1986; Zhang and Cai 1987; Han et al. 1997; Qin et al. 2002). Based on stable isotope systematics (O, H, S) and fluid inclusion evidence of the Lamo Cu–Zn skarn deposit (central ore belt) and the Tongkeng-Changpo polymetallic Sn deposit (western ore belt), Fu et al. (1991, 1993) suggested that the ore-forming fluids were derived from the Longxianggai Granite. Li and Chen (1989), on the other hand, suggested both the Longxianggai Granite and meteoric waters as hydrothermal fluid sources. More recently, Pašava et al. (2003) studied the composition of inclusion fluids and metallogenic conditions of the eastern belt of the Dachang ore field. They suggested that the polymetallic tin ores from the main sulfide stage formed from carbono-aqueous fluids and that black shales played an important role in the origin of these deposits. Zhao et al. (2002) analyzed the He isotopic composition of inclusion fluids in one pyrite sample in the no. 92 stratiform orebody at Tongkeng-Changpo. Their results suggest that mantle fluids may have been involved in ore formation.

Recent mining exposures at the Tongkeng-Changpo mine provided an ideal opportunity for detailed underground investigations and systematic sampling. In this paper, we report the results of our studies of fluid inclusions and He isotopic compositions of samples from different levels of the Tongkeng-Changpo vein, stockwork, and stratiform ores. We suggest that, in addition to magmatic fluids related to the Longxianggai Granite, mantle-derived fluids may also have been involved in the genesis of the Tongkeng-Changpo ore system.

Geologic setting

The Dachang ore field is located in the center of the northwest striking Danchi (or Nandan-Hechi) fold-and-thrust belt, at the border between the Jiangnan anticline and the Tiengui syncline (Figs. 1 and 2). The Danchi belt underwent subsidence and faulting in Devonian–Carboniferous times, and folding in the Middle Triassic. Tectonic activity in the district was dominated by extension and block faulting during the Cretaceous, which also controlled the emplacement of contemporaneous granite intrusions (Chen et al. 1989; Cai et al. 2004). The ore fields in the Danchi fold-and-thrust belt include Mayang (Hg), Mangchang (polymetallic Sn), Dachang (polymetallic Sn), Beixiang (polymetallic Sn), and Wuxu (polymetallic Pb–Zn; Fig. 1). These deposits are hosted in Devonian to Triassic platform sedimentary successions that were intruded and thermally metamorphosed by Yanshanian (Late Mesozoic) granitoids. Several lines of evidence show that the Dachang ore field is spatially and genetically associated with a granitic pluton, with the ore zones lying in the thermally metamorphosed sedimentary rocks above the roof of the pluton (Lattanzi et al. 1989).

In the Dachang area, the sedimentary succession is approximately 2,600 m thick and consists of the Mid-Devonian Nabiao and Luofu Groups, Upper-Devonian Liujiang, Wuzishan and Tongchejiang Groups, and Carboniferous Shimen and Huanglong Groups (Fig. 3). The main structures in the area are the parallel NW-trending Longxianggai anticline and Longxianggai fault and the Dachang anticline and Dachang fault (Fig. 2). Results of a gravity survey indicate that the NW-trending faults possibly reach the lower crust and perhaps even the upper mantle (Cai et al. 2004).

The Longxianggai granite stock is situated in the central part of the Dachang tin field, near the axis of the Longxianggai anticline, covering an area of approximately 0.5 km^2 (Fig. 2). It consists predominantly of biotite granite with subordinate porphyritic granite, and probably belongs to the S-type granite category as defined by Chappell and White (1974), derived from partial melting of continental crust (Chen et al. 1993). The Lamo skarn Cu–Zn ore deposit (Fig. 2) is at the contact zone between the Upper Devonian limestone and the granite. The Tongkeng-Changpo, Bali, Longtoushan, Dafulou, Huile, and Kangma polymetallic tin deposits are sited along the eastern and western margins of the granite stock. On the east and west sides of the Tongkeng-Changpo deposit, a N–S-trending granite porphyry dike (Eastern Dike) and a diorite porphyry dike (Western Dike) along the same trend are present. The SHRIMP (sensitive high-resolution ion microprobe) U–Pb method was used to determine the ages of the Longxianggai granite stock, granite dike, and diorite dike (Cai et al. 2006a). The biotite granite was dated at 93±1 Ma, porphyritic granite at 91±1 Ma, the granite porphyry dike at 91±1 Ma, and the diorite porphyry dike at 91±1 Ma, respectively (Yanshanian thermal event).

Geology of the Tongkeng-Changpo deposit

Geological and structural setting

The Tongkeng-Changpo deposit lies about 4 km southwest of the Longxianggai granite stock (Fig. 2). The most important structures in the Tongkeng-Changpo area are the Dachang anticline, Dachang fault (F_1), and a series of detachment faults developed along lithological contacts. The axis of the Dachang anticline trends 340° and turns to 310° at the mine. The Dachang Fault is in the southwest limb of the Dachang anticline and is parallel with the axis

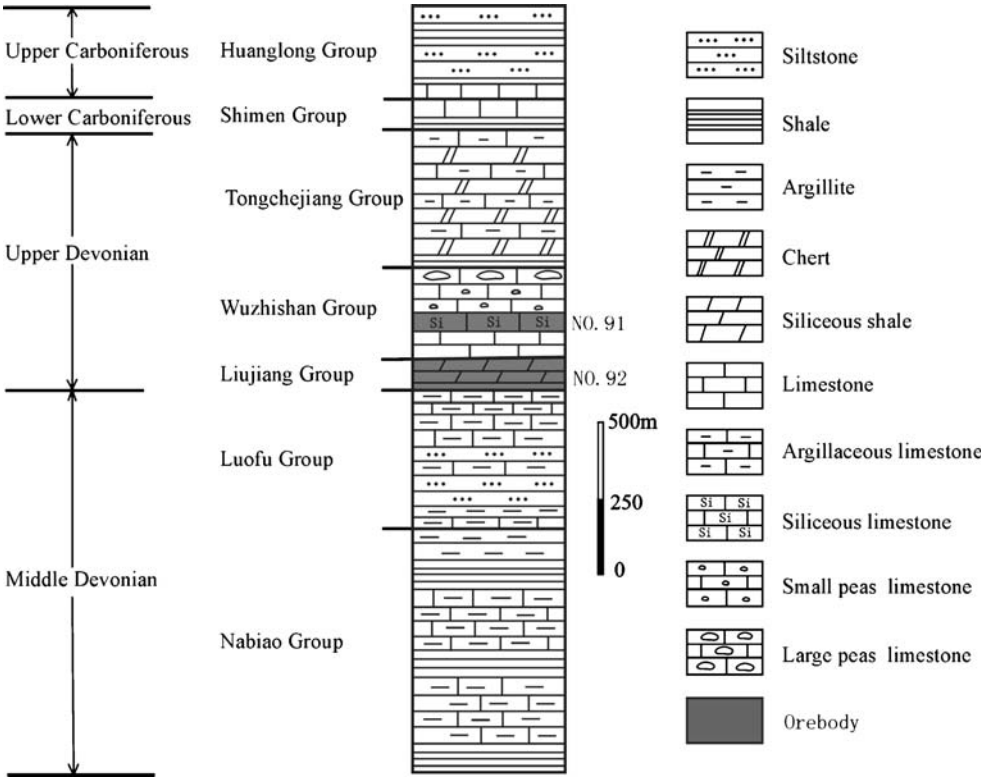

Fig. 3 Stratigraphic column of Dachang ore field

of the anticline (Fig. 2). The detachment fault and subsidiary faults trend are 30°N to 60°E and are the main sites of mineralization.

Orebodies

The orebodies of the Tongkeng-Changpo deposit can be classified into three major types according to their style and shape: veins, stockworks, and stratiform orebodies (Fig. 4).

Vein-style ores are of two types: (1) single, cross-cutting veins and (2) bedding-parallel vein systems. The cross-cutting veins are at the top of the deposit and are mainly located near the axis of the Dachang anticline. They are commonly 0.2 to 1.5 m thick, 50 to 200 m long, and extend to depths of 100 to 300 m. More than 200 veins have been discovered in the Tongkeng-Changpo deposit. The bedding-parallel vein (nos. 75, 77, and 79 ore zones) developed along the detachment fault; they are commonly 0.2 to 3.5 m thick, 50 to 300 m long, and extend to depths of 100 to 250 m. The vein ores contain an average of 7.4% Zn and 2.1% Sn.

Stockworks (nos. I and II) are mainly sited in the flat northeast limb of the Dachang anticline and are hosted by thick bedded limestones. The orebodies consist of numerous fine veins, about 0.5 to 1 cm thick, with a frequency of about 10 to 30 veins/m. The orebodies normally have grades of 1.1% Sn and 2.7% Zn.

Stratiform ores (nos. 91 and 92) are mainly in the northeast limb of the Dachang anticline and are developed along the detachment fault. The no. 91 orebody, situated above the no. 92 orebody, is hosted by the Devonian laminated siliceous limestone of the Wuzhishan Group and is 1,030 m long, with an average thickness of 16 m. The orebody consists of small crosscutting, bedding-plane veins and disseminations (Fig. 5a). Individual veins are commonly 0.5 to 3 cm thick. They are characterized by a high content of sulphides (30% by volume), and high grades of Sn (1.3%) and Zn (4%). The no. 92 orebody, hosted by the Devonian siliceous shale and argillite with calcareous nodules of the Liujiang Group, is 1,130 m long with an average thickness of 26 m. The orebody consists of stockworks as well as disseminations (Fig. 5b). It is characterized by lower grades of Sn (0.8%) and Zn (2.1%).

Mineral paragenesis

The vein, stockwork, and stratiform orebodies have the same mineral assemblage (Fig. 6), although there is much variation in sulphide abundance and grain size. Stage I consists of pyrrhotite, pyrite, sphalerite, with cassiterite, stannite, tourmaline, quartz, and arsenopyrite and is characterized by euhedral quartz and cassiterite crystals. Stage II consists of sphalerite, various sulphosalts, pyrite, pyrrhotite, quartz, and rare cassiterite, marcasite, and calcite. Cassiterite is anhedral and light yellowish in colour. Stage III represents the last mineralization event, consisting of calcite and rare quartz, cassiterite, pyrite, marcasite, and minor sulphosalts.

Stages I and II are the most important mineralization stages in the deposit.

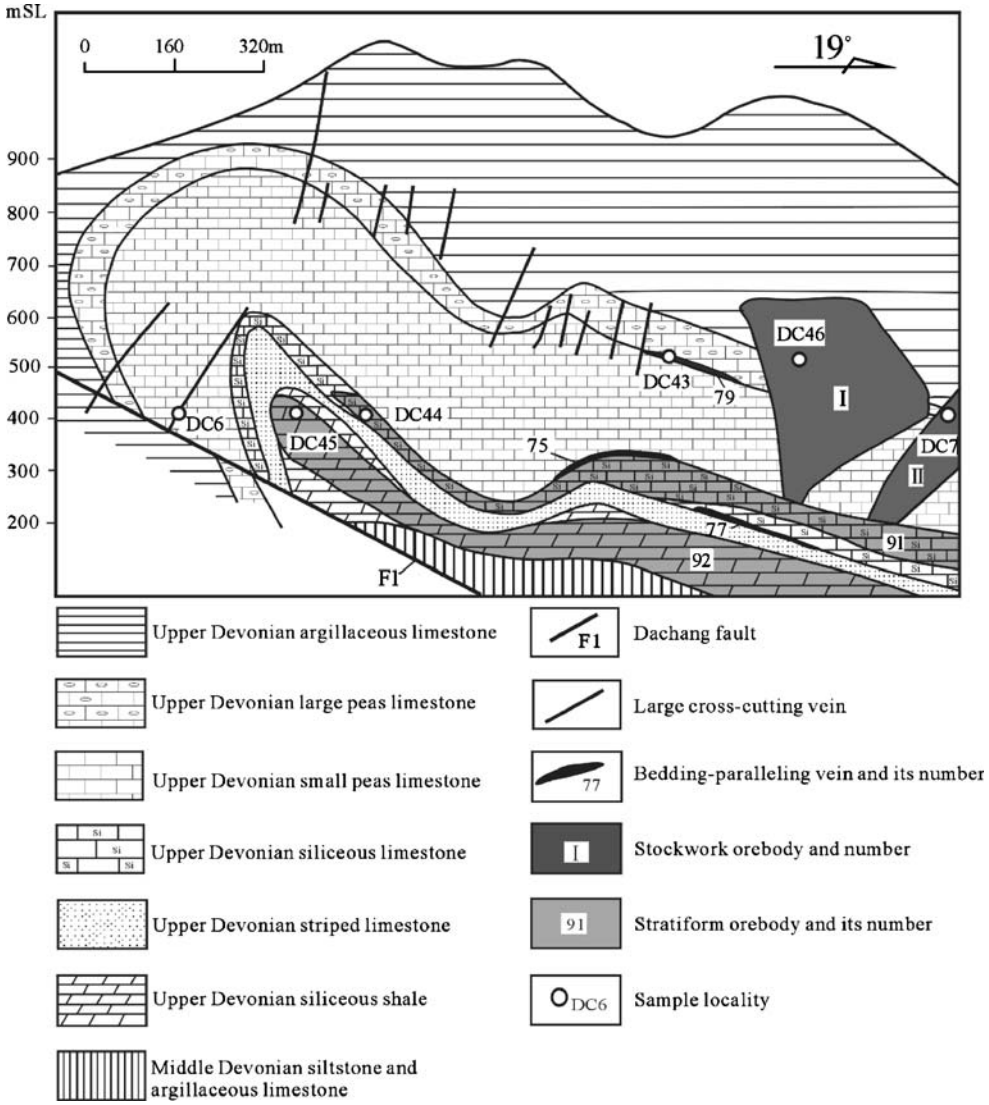

Fig. 4 Geologic cross-section of the Tongkeng-Changpo deposit (compiled from Tongkeng-Changpo mine maps)

Sampling and analytical methods

Thirty samples from the vein-type ore (including cross-cutting veins, bedding-parallel veins and stockworks) and the stratiform orebodies of the Tongkeng-Changpo deposit were collected for mineralogical and microthermometric studies. Of these, 15 samples were chosen for Laser Raman spectroscopy. Microthermometric measurements were carried out on a THMS G600 heating–freezing stage (+600/−196°C) at Yichang Institute of Geology and Mineral Resources, China Geological Survey. The heating rate was 0.1 to 0.2°C/min between 0 to 10°C and below −56.6°C with an accuracy of ±0.1°C, about 3 to 5°C/min between 10 to 31°C and 5 to 10°C/min at higher temperatures with an accuracy of about ± 2°C. The Laser Raman spectroscopic analysis was conducted at the Institute of Mineral Resources, Chinese Academy of Geological Sciences (CAGS), using the RM2000 laser Raman spectroscope (British Renishaw). The analytical conditions are: Ar^{+} laser instrument using laser beam of 514.5-nm wavelength with a 20-mW power, resolution of 1 to 2 cm^{-1}, and range of scan from 4,000 to 100 cm^{-1}. The smallest diameter of the laser beam was 1 μm.

Pyrite is known to be a suitable trap for noble gases (Stuart et al. 1994; Jean-Baptiste and Fouquet 1996; Burnard et al. 1999), particularly because it is able to retain helium over long periods of geologic time, in contrast to quartz and feldspar (Mark Kendrick, written communication 2002). We selected six pyrite samples for He isotope analysis: two samples each from the vein, stockwork, and stratiform orebodies. Sample location is shown in Fig. 4. All samples were prepared and analyzed at the Isotope Laboratory, Institute of Mineral Resources, CAGS.

The helium and argon isotope compositions were analyzed by bulk extraction of fluids using the vacuum crushing method. This method can reduce the effects from in-situ-produced radiogenic isotopes and adsorbed atmospheric gases, overcoming problems because of low blank. In addition, the larger fluid volumes, relative to laser

Fig. 5 **a** No. 91 orebody (455-m level). The host rock is laminated siliceous limestone. The ore consists of small crosscutting NE-trending and bedding-parallel veins. **b** No. 92 orebody (455-m level). The host rock is siliceous shale and argillite with calcareous nodules. The ore consists of small crosscutting and bedding-parallel veins

extraction methods, allow for greater precision in the data. The pure pyrite separates, 0.2 to 0.8 mm in size, were first washed ultrasonically in distilled water, then in acetone, and finally oven dried. The online screw-type crushers were constructed from modified vacuum valves. Six samples, about 1 g each, were loaded into the crushers at the same time. The samples were baked at 100 to 150°C for 24 h to remove adsorbed atmospheric gases before crushing.

The gases released by crushing were exposed to a titanium sponge pump at 780°C and a zircon-aluminum pump at 300°C for 20 min to remove the active gases, such as H_2, N_2, O_2, CO_2, CH_4, and H_2O, and any organic substances. Then, the remaining gases were exposed to a second cold zircon-aluminum pump for 10 min, and argon was condensed onto liquid N_2-cooled charcoal for 10 min. Comparatively purer helium travels directly into the analyzing system of the mass spectrometer. Trace impure gases such as hydrogen, which entered the system along with the helium, were removed by a liquid N_2-cooled titanium sublimation pump located adjacent to the spectrometer ion source.

Mineral	Stage I	Stage II	Stage III
Tourmaline	—		
Quartz	—	—	—
Cassiterite	—	—	–
Stannite	–		
Arsenopyrite	—	—	
Pyrrhotite	—	—	
Pyrite	—	—	—
Sphalerite	—	—	
Marcasite		—	—
Sulphosalts		—	—
Calcite		—	—

Fig. 6 Mineralization stages and paragenesis in the Tongkeng-Changpo deposit (*thick*, *medium-thick*, and *thin bars* represent major, minor, and rare contents of minerals in individual stages, respectively)

The helium isotope compositions were measured on a MI-1201IG inert gas mass spectrometer made by "SELMI" based in Sumy, Ukraine. A Faraday cup was used to measure ^{4}He, and ^{3}He was measured on an electron multiplier. The mass resolution of 1,200 enables ^{3}He to be distinguished from the HD-H_3 doublet peak. Argon was adsorbed from the charcoal finger and separated from xenon at −78°C. The ^{40}Ar was measured by a Faraday cup and ^{36}Ar and ^{38}Ar by an electron multiplier. A standard was measured before analyzing the samples, and the results from the samples were normalized to the standard, which was made by purified air and periodically examined during its use. All the analytical results are based on the internationally accepted values for atmospheric ^{3}He/^{4}He of 1.4×10^{-6}, and ^{40}Ar/^{36}Ar of 295.5. Helium results are reported as R/Ra ratios, where R is the ^{3}He/^{4}He ratio of the sample and Ra is that of the modern atmosphere. The hot blank level of ^{4}He was 2×10^{-11} cm^3 STP for which ^{3}He/^{4}He ratio of 1×10^{-6} was assumed, whereas the blank level of ^{40}Ar was 5×10^{-9} cm^3 STP/g. The effect of the blank on the measured ratio is negligible. The analytical precision of standard gas was 1%.

Fluid inclusion studies

Types of fluid inclusions and their features

Quartz intergrown with cassiterite is the main transparent mineral in the ores and contains abundant primary and pseudosecondary fluid inclusions (Roedder 1984). These fluid inclusions have relatively regular shapes (negative crystal or incomplete negative crystal shapes) or occur along microfractures within quartz grains, but do not cut or cross crystal boundaries. Fluid-inclusions-forming groups usually have similar degrees of infill and homogenization temperatures, as well as relatively consistent compositions. The primary and pseudosecondary fluid inclusions in quartz

may be classified as CO_2-type and NaCl-H_2O-type base upon their phase relationship and chemical composition at room temperature.

CO2-type fluid inclusions

The CO_2-type fluid inclusions commonly contain a significant, but quite variable amount of CO_2. They have relatively regular shapes (usually negative crystal or incomplete negative crystal shapes) and are about 3 to 40 μm (mainly 5–15 μm) in diameter. The CO_2-type inclusions are mainly in quartz formed during mineralization stages I and II (Fig. 7). Based on the number of phases in inclusions at room temperature, CO_2-type fluid inclusions may be subdivided into two subtypes: three-phase (A-1 subtype) and two-phase (A-2 subtype).

A-1 subtype Three-phase CO_2-rich inclusions consist of vapour-rich V_{CO_2} and liquid-rich L_{CO_2} and L_{H_2O} (Fig. 8a,b). The volume of the CO_2 phase in the fluid inclusions varies greatly, accounting for 22 to 70% of the bubbles.

A-2 subtype Two-phase CO_2-type inclusions (Fig. 8c,d) consisting of L_{CO_2} and L_{H_2O} are much less common. The volume of the CO_2 phase in the fluid inclusions also varies greatly, accounting for 20 to 80% of the bubbles.

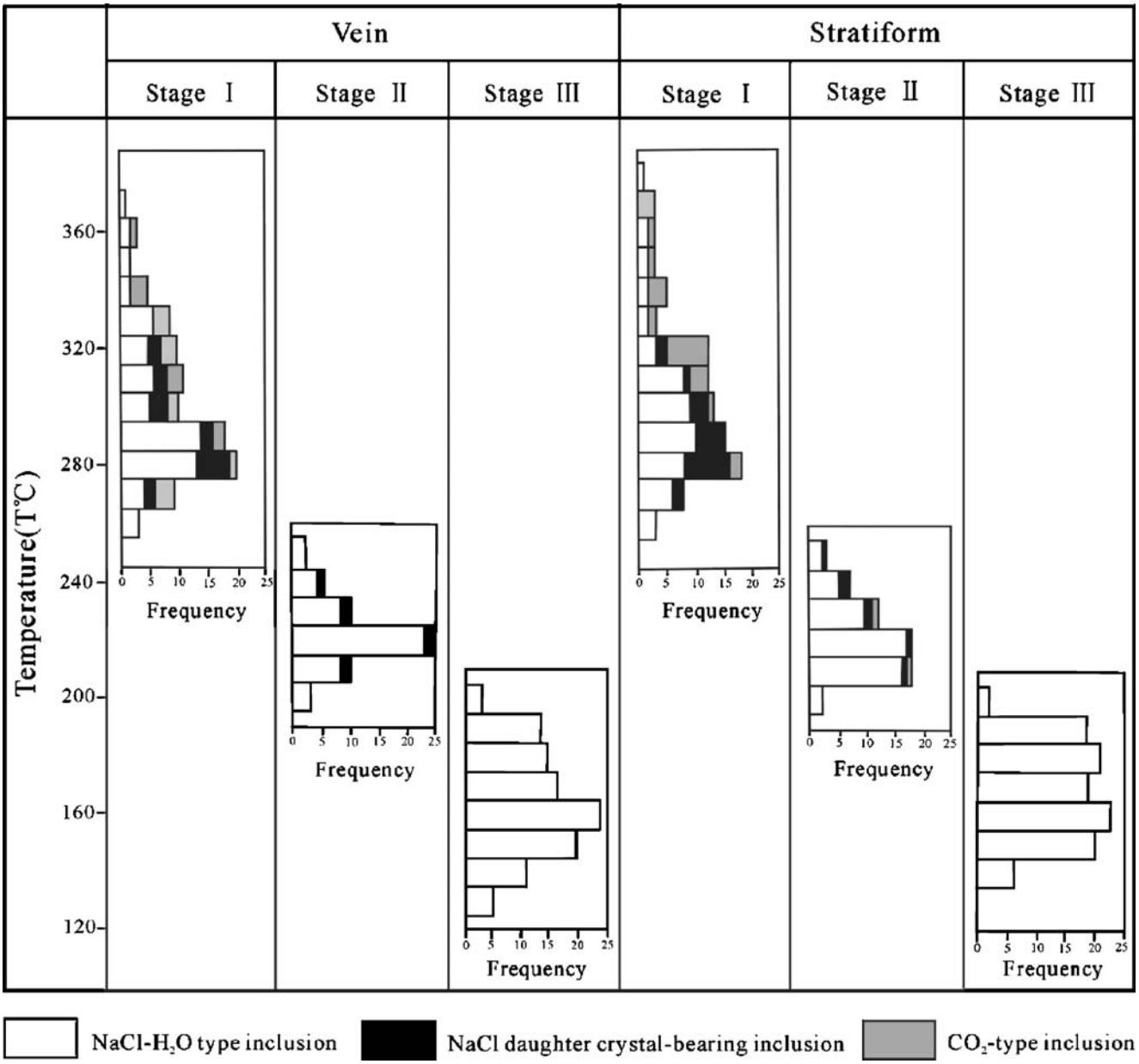

Fig. 7 Histogram of homogenization temperatures (Th_{total}) of various types of inclusions

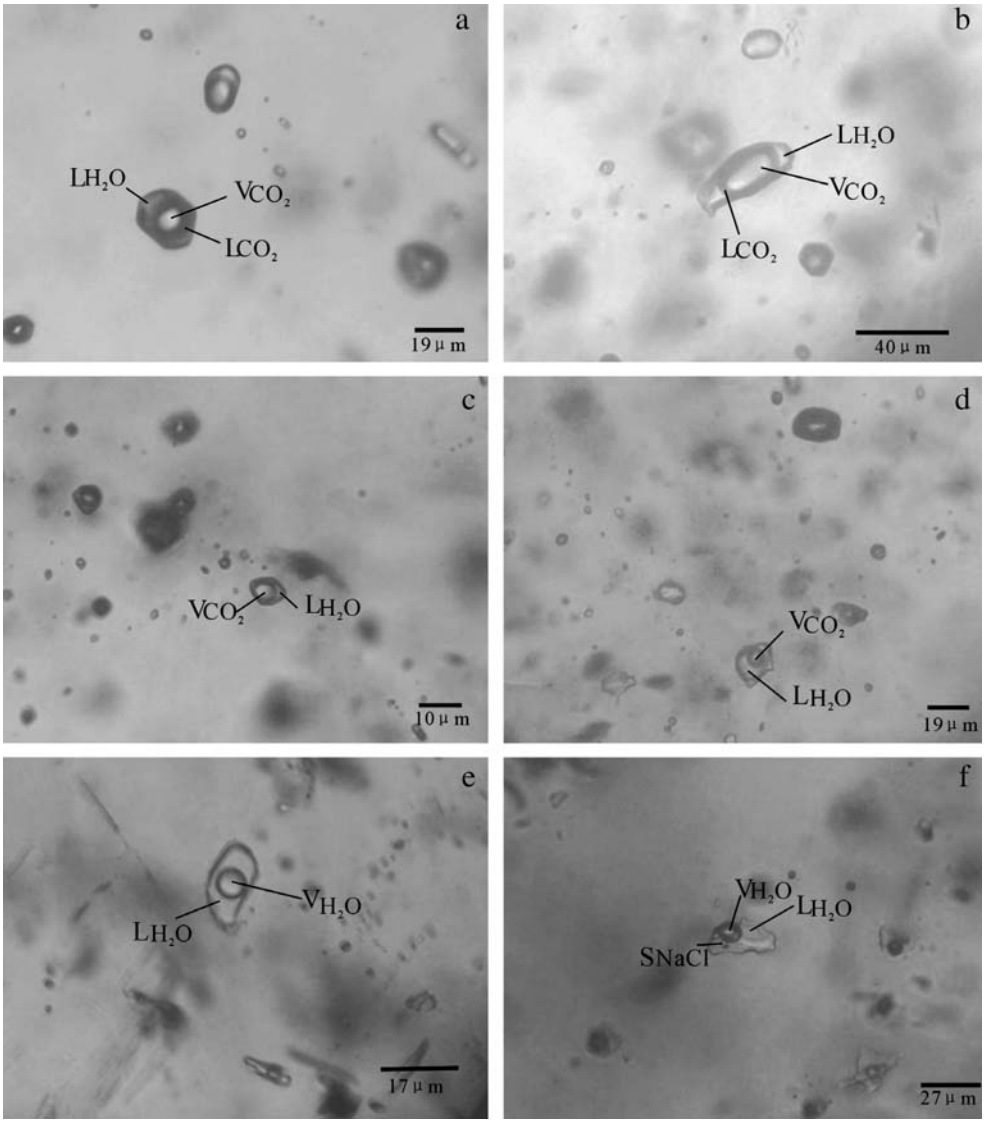

Fig. 8 Photomicrographs of fluid inclusion types in the Tongkeng-Changpo deposit. **a**, **b** The variable phase ratios of three-phase CO_2-type inclusions in quartz. **c**, **d** The variable phase ratios of two-phase CO_2-type inclusions in quartz. **e** A two-phase NaCl-H_2O-type inclusion in quartz. **f** A NaCl daughter crystal-bearing fluid inclusion in quartz

NaCl-H2O-type fluid inclusions

NaCl-H_2O fluid inclusions consist mainly of NaCl and H_2O. Most coexist with the CO_2-type inclusions and may be subdivided into one- (B-1 subtype), two- (B-2 subtype, Fig. 8e), or multiphase (B-3 subtype, Fig. 8f) inclusions.

B-1 type Single-phase fluid inclusions of L_{H_2O} occur mainly in quartz formed during stage III. They have rectangular, rhombic, or polygonal shapes and are distributed randomly or along microfractures but do not transect crystal boundaries. The size of fluid inclusions varies greatly, with less than 1 up to 40 μm in length. This type of fluid inclusion is rarely observed.

B-2 subtype Two-phase fluid inclusions are the most common and usually coexist with the CO_2-type inclusions. They are either liquid-rich L_{H_2O} or vapor-rich V_{H_2O} and contain vapor bubbles up to 10–80% by volume. They are about 3 to 40 μm (mainly 5–15 μm) in diameter and occur randomly in clusters in quartz of all three hydrothermal stages.

B-3 subtype Multiphase daughter mineral-bearing inclusions are high-salinity aqueous fluid inclusions. They are rare and have a random distribution. The size of the daughter crystals is typically close to that of the vapor bubble. Microscopic study suggests that most daughter crystals are halite.

Microthermometric measurements and results

CO2-type inclusions

A total of 46 CO_2-type inclusions were measured in 15 samples from vein-type and stratiform orebodies. These data are summarized in Table 1.

Table 1 Microthermometric data for CO_2-type inclusions in quartz

Sample no.	Type of orebody	t_{mCO_2} (°C)	T_{mcl} (°C)	Th_{CO_2} (°C)		Th_{total} (°C)		Salinity (wt%NaCleq.)	Density (g/cm^3)			ϕ% CO_2	$x_{(CO_2)}$	$x_{(H_2O)}$	$x_{(NaCl)}$
				V → L	L → V	H_2O	CO_2		CO_2	H_2O	Total				
TK405-15	Stratiform	−58.0	7.0	28.0		310		5.77	0.653	0.757	0.726	30	0.16	0.824	0.016
		−59.0	7.6		27.0		330	4.69	0.266	0.704	0.397	70	0.29	0.699	0.011
		−59.0	7.7		27.5		345	4.51	0.274	0.694	0.400	70	0.30	0.690	0.010
		−56.7	7.8	28.5		370		4.32	0.642	0.626	0.631	33	0.20	0.789	0.011
TK405-31	Vein	−58.0	0.8		28.0		320	14.67	0.282	0.847	0.452	70	0.27	0.693	0.037
		−57.0	5.0	28.0		310		9.08	0.653	0.803	0.754	33	0.15	0.823	0.027
		−58.0	1.0		22.5		320	14.44	0.212	0.840	0.388	72	0.24	0.722	0.038
TK355-4	Stratiform	−58.5	9.1	21.0		310		1.83	0.755	0.712	0.729	40	0.25	0.746	0.004
		−59.5	9.3		19.0		335	1.43	0.183	0.654	0.324	70	0.24	0.757	0.003
		−59.0	9.0	29.0		300		2.03	0.630	0.734	0.700	33	0.17	0.825	0.005
		−59.5	9.2		19.5		340	1.63	0.186	0.730	0.431	55	0.14	0.856	0.004
TK355-1	Stratiform	−59.0	6.0	23.5		210		7.48	0.724	0.913	0.866	25	0.12	0.859	0.021
TK554-2	Vein	−56.8	8.3	22.0		310		3.38	0.743	0.730	0.735	35	0.21	0.782	0.008
		−56.8	8.3	21.5		300		3.38	0.749	0.767	0.761	33	0.19	0.801	0.009
		−57.0	8.8		22.0		320	2.42	0.208	0.691	0.353	70	0.25	0.744	0.006
		−57.0	8.8		22.5		325	2.42	0.212	0.678	0.352	70	0.26	0.734	0.006
TK505-5	Stratiform	−56.7	9.3	25.5		280		1.43	0.696	0.771	0.743	38	0.21	0.786	0.004
		−57.0	9.7		28.0		365	0.62	0.282	0.512	0.351	70	0.37	0.629	0.001
		−56.7	8.2	27.5		360		3.57	0.662	0.629	0.637	23	0.14	0.850	0.010
		−56.7	8.2		20.5		365	3.57	0.194	0.616	0.300	75	0.30	0.692	0.008
TK505-7	Vein	−56.8	9.3	26.0			322	1.43	0.688	0.684	0.687	70	0.51	0.488	0.002
		−56.7	8.0	28.5		300		3.95	0.642	0.755	0.732	20	0.10	0.889	0.011
		−56.9	8.7	29.0		360		2.62	0.630	0.604	0.613	33	0.20	0.793	0.007
TK505-15	Stratiform	−58.5	3.5	29.0		315		11.29	0.630	0.796	0.743	32	0.16	0.808	0.032
		−58.5	8.5		28.0		320	3.00	0.282	0.701	0.408	70	0.30	0.693	0.007
		−56.8	3.8	28.5		280		10.87	0.642	0.858	0.815	20	0.09	0.877	0.033
TK505-16	Stratiform	−59.5	9.3		27.5		330	1.43	0.274	0.659	0.390	70	0.31	0.687	0.003
		−59.0	8.7	27.4		230		2.62	0.664	0.850	0.789	33	0.16	0.833	0.007
		−56.8	9.1	27.6		330		1.83	0.662	0.664	0.663	28	0.16	0.835	0.005
TK483-3	Vein	−56.8	7.5	26.5		335		4.87	0.680	0.700	0.690	50	0.31	0.679	0.011
		−57.0	8.5		27.5		310	3.00	0.274	0.725	0.409	70	0.29	0.703	0.007
		−56.8	7.5		26.0	340		4.87	0.252	0.693	0.473	50	0.15	0.837	0.013
		−56.7	7.5	28.0		320		4.87	0.653	0.725	0.709	22	0.12	0.866	0.014
TK455-3	Vein	−56.7	4.0		27.5		340	10.58	0.274	0.763	0.430	68	0.26	0.714	0.026
		−56.8	8.0	28.5		315		3.95	0.642	0.725	0.707	22	0.12	0.869	0.011
		−56.7	9.0	29.0		320		2.03	0.630	0.691	0.676	25	0.13	0.865	0.005
TK455-15	Vein	−56.8	6.3	24.0		270		6.97	0.717	0.834	0.797	32	0.17	0.811	0.019
		−56.8	6.3	23.0		268		6.97	0.731	0.830	0.798	32	0.17	0.811	0.019
		−56.7	6.0	26.5		270		7.48	0.680	0.839	0.804	22	0.11	0.868	0.022
TK455-19	Stratiform	−57.5	9.5	23.5		290		1.03	0.724	0.743	0.737	30	0.17	0.827	0.003
		−58.0	9.0		27.5		340	2.03	0.274	0.646	0.348	80	0.43	0.566	0.004
DC05	Vein	−57.0	8.5	24.5		285		3.00	0.710	0.772	0.752	32	0.18	0.812	0.008
		−58.0	9.5		22.5		290	1.03	0.212	0.743	0.371	70	0.24	0.758	0.002
		−56.8	6.1	26.0		280		7.31	0.688	0.824	0.749	22	0.11	0.869	0.021
DC37	Stratiform	−59.5	3.5	25.5		305		11.29	0.696	0.826	0.784	32	0.16	0.808	0.032
		−59.6	4.8		18.5		320	9.39	0.180	0.787	0.362	70	0.21	0.765	0.025

t_{mCO_2} melting temperature; T_{mcl} melting temperature of CO_2 clathrate; $x_{(CO_2)}$ partial homogenization temperature of CO_2; Th_{total} total homogenization temperature; ϕ volume of CO_2; $x_{(CO_2)}$, $x_{(H_2O)}$, and $x_{(NaCl)}$ are mole fractions of CO_2, H_2O, and NaCl in CO_2-type inclusions, respectively; *V* vapor phase; *L* liquid phase

The melting temperatures of CO_2 typically range from −56.7 to −59.6°C, slightly below the triple point of pure CO_2 (−56.6°C; Roedder 1984), indicating that only a minor amount of other volatiles such as CH_4 is present in the vapor phase (Diamond 2001). The clathrate melting temperatures obtained from analyses of fluid inclusions range from 1.0 to 9.7°C. Using the equation of Bozzo et al. (1973), neglecting the effect of minor methane, the

salinities of CO_2-type inclusions range from 0.62 to 14.67 wt.% NaCl equiv., with the majority between 1 and 7 wt.% NaCl equiv. Using final homogenization temperatures (Table 1) and the above salinities, we can obtain the densities of the aqueous (ρH_2O) phase (Liu and Shen 1999). These range from 0.668 to 0.826 g/cm^3 (Table 1).

The CO_2 homogenization temperatures for the 46 CO_2-type fluid inclusions range from 18.5 to 29.0°C, 18 of them homogenized to vapor when heated and the other 28 to liquid. Given the homogenization temperatures, the corresponding CO_2 densities can be calculated (Liu and Shen 1999). The density data of the CO_2 phase can be classified into two groups as shown in Table 1, i.e., a low-density group between 0.180 and 0.282 g/cm^3, and a high-density group between 0.630 and 0.755 g/cm^3.

The CO_2-type fluid inclusions were homogenized to H_2O-rich liquid at a temperature of 210 to 370°C, with a frequency peak ranging from 275 to 365°C, and homogenized to CO_2-rich vapor at temperatures ranging from 280 to 365°C. Both the H_2O-rich and CO_2-rich inclusions have a similar range of homogenization temperatures, indicating that these fluid inclusions were trapped under similar temperature conditions during ore formation.

The total density, $x(CO_2)$, x(NaCl), and $x(H_2O)$ of CO_2-type inclusions is calculated by the formula given by Liu and Shen (1999). The total density of H_2O-rich and CO_2-rich inclusions is between 0.613 and 0.866 g/cm^3, and 0.300 to 0.473 g/cm^3, respectively. The calculated $x_{(CO_2)}$ is between 0.09–0.51, $x_{(NaCl)}$ 0.001–0.038, and $x_{(H_2O)}$ 0.488–0.889 (Table 1), based on the formulae of Liu and Shen (1999).

NaCl-H2O-type fluid inclusions

Thirty two-phase NaCl-H_2O-type fluid inclusions and five daughter-bearing multiphase NaCl-H_2O-type fluid inclusions from 20 samples were studied in detail. The initial melting point of two-phase NaCl-H_2O-type fluid inclusions is 20.8°C.

The temperature of fluid inclusions that homogenized to liquid is in the range of 130 to 360°C, whereas those homogenized to vapor have a range of 225 to 320°C (Table 2).

The salinity of the two-phase NaCl-H_2O inclusions can be obtained from the final ice melting temperature in the light of data for the NaCl-H_2O system proposed by Bodnar (1992). The salinity ranges from 2.90 to 11.34 wt.% NaCl equiv., with the majority between 3 to 10 wt.% NaCl equiv. (Table 2), which corresponds well to the salinity of CO_2-type inclusions. According to the list of melting temperature of NaCl daughter minerals vs. their corresponding salinities provided by Liu and Shen (1999), the salinity of daughter-bearing multiphase inclusions ranges from 29.66 to 35.99 wt.% NaCl equiv.

The density of fluid inclusions is estimated from the homogenization temperature and the salinity obtained from the table of pressure–temperature–composition–density for the NaCl-H_2O system (Liu and Shen 1999). The density of two-phase NaCl-H_2O-type fluid inclusions ranges from 0.744 to 0.974 g/cm^3 (Table 2), and that of daughter-bearing multiphase NaCl-H_2O inclusions ranges from 0.998 to 1.093 g/cm^3.

The histogram of Fig. 7 depicts the homogenization temperature of all types of fluid inclusions from the Tongkeng-Changpo deposit. The homogenization temperature exhibits three groups of high-, medium-, and low-temperature values, ranging from 270 to 365°C, 210 to 240°C, 140 to 190°C, respectively. These correspond to the three ore-forming stages (I, II, III). There are two types of fluid inclusions at the high- and middle-temperature stages (CO_2- and NaCl-H_2O), whereas the fluid inclusions from the low-temperature stage are only of the NaCl-H_2O-type.

He isotope composition of inclusion fluids

The helium isotope compositions of the inclusion fluids in pyrite are presented in Table 3. Previous studies have demonstrated that He loss from fluid inclusions trapped in pyrite is insignificant (Stuart et al. 1994). The pyrite samples analyzed were well-formed euhedral crystals with no evidence of subsequent deformation and show a paragenesis with sphalerite, sulphosalts, cassiterite, pyrrhotite, arsenopyrite, and quartz. Therefore, we are confident that the extracted fluids were related to the mineralization.

The $^3He/^4He$ ratios are quite constant in a range of 1.61×10^{-6} to 4.12×10^{-6}, 1.64×10^{-6} to 2.19×10^{-6}, and 2.27×10^{-6} to 3.50×10^{-6} for pyrite from veins, stockworks, and stratiform orebodies, respectively (Table 3). There is no significant difference in the content of typical radiogenic ^4He and $^3He/^4He$, suggesting that the different ore types analyzed have the same fluid source.

Discussion

Characteristics of ore-forming fluids

The volumetric proportion of CO_2 in CO_2-type fluid inclusions, formed in stages I and II, is between 20 and 80%. CO_2-type inclusions are commonly associated with two-phase NaCl-H_2O inclusions and daughter mineral-bearing multiphase inclusions, which were all trapped during the same stage (Fig. 7). CO_2-rich-type fluid inclusions homogenized to CO_2 with a homogenization temperature between 280 and 365°C; H_2O-rich inclusions homogenized to NaCl-H_2O phase with a homogenization temperature between 210 and 370°C, with peaks at 275 and 365°C. These two kinds of inclusions exhibit differences in

Table 2 Microthermometric data for two-phase NaCl-H_2O-type fluid inclusions in quartz

Sample no.	Type of orebody	t_{fl} (°C)	Th_{total}/°C		Salinity [w%(NaCleq.)]	Density (g/cm^3)	V_{H_2O} (%)
			V → L	L → V			
TK455-2	Vein	−2.7	170		4.49	0.931	12
TK455-15	Vein	−4.1	140		6.59	0.974	15
TK455-26	Vein	−6.9	220		10.36	0.926	18
		−3.9		280	6.30	0.814	75
TK455-27	Vein	−2.9	130		4.80	0.969	10
		−3.3		225	5.41	0.879	80
TK631-2	Vein	−3.8	170		6.16	0.944	15
TK554-2	Vein	−2.3	165		3.87	0.931	12
		−3.5	195		5.71	0.915	20
TK505-5	Stratiform	−2.8	150		4.65	0.951	12
TK505-7	Vein	−4.0	210		6.45	0.905	15
		−4.0	230		6.45	0.882	20
TK505-16	Stratiform	−2.1	200		3.55	0.893	18
TK505-18	Vein	−5.7	215		8.81	0.919	12
TK483-3	Vein	−3.0	155		4.96	0.948	12
TK483-4	Vein	−1.7	170		2.90	0.920	15
TK405-8	Stratiform	−2.5	185		4.18	0.914	12
TK405-16	Vein	−6.5	280		9.86	0.849	12
		−6.7	275		10.11	0.858	10
		−6.0	310		9.21	0.795	15
		−7.5		300	11.10	0.832	68
		−7.7		320	11.34	0.803	75
TK405-19	Stratiform	−2.8	155		4.65	0.946	10
		−1.7	205		2.90	0.882	15
TK355-1	Stratiform	−3.9	210		6.30	0.904	12
DC3	Stratiform	−1.8	145		3.06	0.944	15
DC37	Stratiform	−6.5	170		9.86	0.972	12
DC47	Stratiform	−4.5	245		7.17	0.875	20
DC60	Stratiform	−6.5	340		9.86	0.761	20
		−6.5	360		9.86	0.744	25

T_{fl} ice melting temperature; Th_{total} total homogenization temperature; V_{H_2O} volume of vapor phase; V vapor phase; L liquid phase.

vapor to liquid ratios, but have similar homogenization temperature. These characteristics are consistent with fluid immiscibility as described by Roedder (1984) and Zhang and Chen (1993), suggesting that the fluid separation of CO_2 and NaCl-H_2O took place during an early stage. The homogenization temperatures of the daughter mineral-bearing multiphase inclusions and two-phase NaCl-H_2O inclusions range from 210 to 385°C, with peaks at 270 and 365°C, indicating that unmixing of fluids (i.e., boiling) had taken place during the early ore-forming stages. Cassiterite in the Tongkeng-Changpo ore deposit was precipitated at an early stage (Fig. 6; Ding et al. 1988; Li and Chen 1989),

Table 3 He, Ar, and S isotopic data of pyrite samples from the Tongkeng-Changpo deposit

Sample no.	Minerals	Type of orebody	$^3He/^4He\times10^{-6}$	$^4He\times10^{-6}$ (cm^3 STP/g)	$^{40}Ar/^{36}Ar$	$^{40}Ar\times10^{-7}$ (cm^3 STP/g)	R/Ra	$^{40}Ar/^4He$
DC6	Pyrite	Large vein	1.61±0.09	6.71	283±1	18.74	1.2	0.28
DC7	Pyrite	Stockworks	1.64±0.27	2.75	273±1	4.84	1.2	0.18
DC46	Pyrite	Stockworks	2.19±0.17	1.72	286±1	2.12	1.6	0.12
DC43	Pyrite	Bedding-parallel vein (79)	4.12±0.37	1.03	305±1	2.17	2.9	0.21
DC44	Pyrite	Stratiform orebody (91)	2.99±0.56	1.77	327±1	6.93	2.1	0.39
DC45	Pyrite	Stratiform orebody (92)	2.27±0.33	1.55	283±1	4.30	1.6	0.28
T38[a]	Pyrite	Stratiform orebody (92)	3.50±0.10	3.67	323±2	24.04	2.5	0.65

[a] Data of sample from Zhao et al. (2002).

and therefore, it is reasonable to conclude that boiling is responsible for the precipitation of cassiterite.

The CO_2-rich and H_2O-rich inclusions formed at stages I and II and were trapped from CO_2-bearing low-saline aqueous solutions during mineralization, whose homogenization temperature may represent the ore-forming temperature. Therefore, it can be concluded that the ore-forming temperature range of mineralization stage I is 270 to 365°C, 210 to 240°C for stage II, and 140 to 190°C for stage III (Fig. 7).

In addition, the composition of inclusion fluids, as detected by Laser Raman spectroscopy, shows that stages I and II are dominated by CO_2 and NaCl-H_2O, with minor amounts of CH_4 and H_2S. The molar percentage of CO_2 in the fluids is between 9–51%, with densities of 0.324–1.093 g/cm^3 and salinities of up to 36.0 wt.% NaCl equiv., but dominantly between 1 and 7 wt.%. The composition of fluids of the late ore-forming stage (stage III) is dominated by NaCl-H_2O, with densities of 0.893–0.972 g/cm^3 and salinities of up to 10 wt.% NaCl equiv., but mainly between 3–7 wt.%. Whereas the CO_2 content of the ore fluids changed during their evolution, the salinity remained more or less constant.

Origin of ore-forming fluids

Experiments on inclusion fluids have shown that the composition of mantle-derived fluids is mainly constrained by fo_2. When fo_2 approaches the QFM (quartz–fayalite–magnetite) buffer conditions, the composition of upper-mantle fluids may be dominated by CO_2 and H_2O (Rui et al. 2003). The mineralization of the Tongkeng-Changpo ore deposit took place within a hydrothermal field in which fo_2 is near the QFM buffer (Fu et al. 1993), the CO_2-rich inclusions of the early stage are dominated by CO_2 and H_2O, showing a composition similar to upper-mantle fluids. The molar fraction of CO_2 ($x_{(CO_2)}$) ranges from 9 to 51%, which is different from the same type of inclusions at the Lamo skarn-type Zn–Cu deposit, where $x_{(CO_2)}$ of ore-forming fluids, derived from the S-type granite stock, is generally lower than 10% (Li and Chen 1989). The study by Fu et al. (1993) also indicated that the ore-forming fluids related to skarn-type Zn–Cu mineralization are characterized by minor CO_2, whereas the fluids in the Tongkeng-Changpo ore deposit are dominated by CO_2. The above data suggest that the CO_2-rich fluids may derive from the mantle, or from a mixture of mantle fluids and magmatic fluids.

As suggested by Giggenbach (1986), isotopes of noble gases may be valuable discriminators to distinguish between mantle, crustal, and meteoric sources. The helium isotope composition is a useful tool for tracing the origin of fluids, which in geological materials have at least three end-members (Simmons et al. 1987; Stuart et al. 1995; Hu et al. 1999; Burnard et al. 1999): (1) air-saturated meteoric water, with a ratio of $^3He/^4He$ of about 1.4×10^{-6} (Ra); (2) mantle fluids, characterized by high content of ^3He with a ratio of $^3He/^4He$ usually in the range of 6 to 9 Ra; (3) radiogenic He from the crust, with ratios of $^3He/^4He$ less than or equal to 0.1 Ra, and a peak between 0.01 and 0.05 Ra.

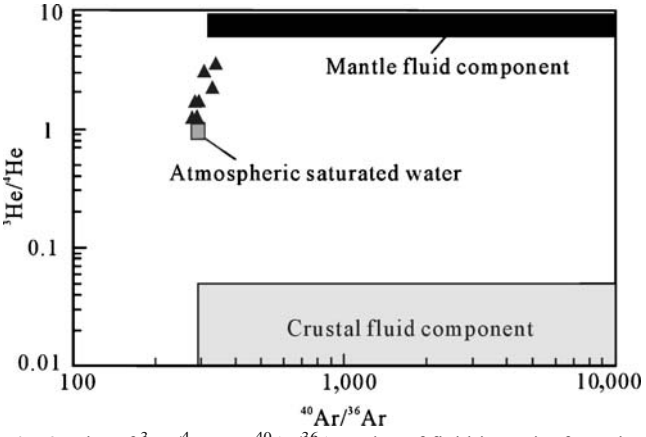

Fig. 9 Plot of $^3He/^4He$ vs. $^{40}Ar/^{36}Ar$ ratios of fluid in pyrite from the Tongkeng-Changpo deposit

As compared with air (1.4×10^{-6} Ra), the $^3He/^4He$ values for pyrite of the Tongkeng-Changpo deposit are within the range of 1.2 to 2.9, 1.2 to 1.6, and 1.6 to 2.5 Ra for veins, stockworks, and stratiform orebodies, respectively. The ratios of $^3He/^4He$ are lower than mantle values, but much higher than continental crust, suggesting that He in the ore-forming fluids is not only from the crust, but also from the mantle. The diagrams of $^3He/^4He$ vs. $^{40}Ar/^{36}Ar$ (Fig. 9) and $^3He/^4He$ vs. $^{40}Ar/^4He$ (Fig. 10) show that the He–Ar isotope compositions have a positive relationship, indicating that the ore-forming fluids represent a mixture of both mantle and crustal sources (Hu et al. 1998).

Ore genesis

The characteristics of inclusion fluids and He isotope systematics of vein-type and stratiform orebodies are

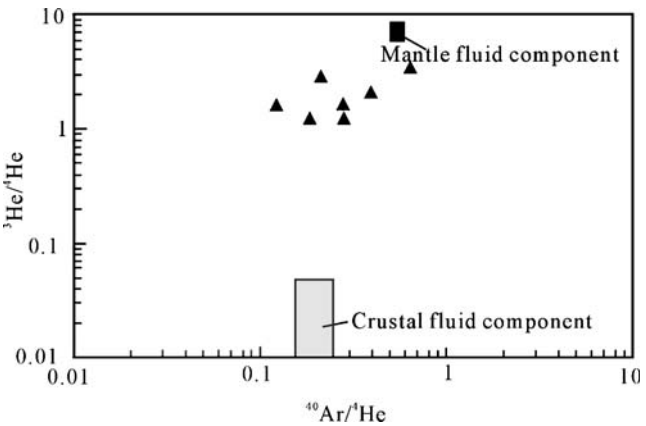

Fig. 10 Plot of $^3He/^4He$ vs. $^{40}Ar/^4He$ ratios of fluid in pyrite from the Tongkeng-Changpo deposit

similar and indicate that the vein-type and stratiform orebodies share the same source and ore-forming processes.

Recently, Wang et al. (2004) presented new $^{40}Ar/^{39}Ar$ data on quartz from the stratiform ores in the no. 91 orebody, giving a plateau age of 94.52±0.33 Ma. The Rb–Sr isochron dating of fluid inclusions of quartz from the no. 92 orebody gave 93.4±1.3 Ma (Cai et al. 2006b). These ages are in accordance with the SHRIMP U–Pb zircon age of the Longxianggai biotite granite of 93±1 Ma (Cai et al. 2006a) showing that there is a close temporal relationship between mineralization and granite emplacement.

The range of $^{3}He/^{4}He$ ratios of 1.2 to 2.9 Ra, i.e., notably higher than crustal fluids, together with the CO_2-rich fluid composition, point to mantle fluids involved in the ore formation of the Tongkeng-Changpo polymetallic tin deposit. The northwest-striking Dachang fault may reach into the lower crust or upper mantle (Cai et al. 2004) and would provide a favorable geological environment for mantle fluids to take part in mineralization.

Acknowledgements We are grateful to Huang Huiming, Wu Decheng, and Wei Keli for their kind help during field work. We also thank Dr. Fan Hongrui for his constructive suggestions on earlier versions of the manuscript. We wish to express our sincere appreciation to Pierfranco Lattanzi, Georges Beaudoin, and Bernd Lehmann for their constructive criticism. Franco Pirajno publishes with the permission of the Executive Director of the Geological Survey of Western Australia.

References

Bodnar RJ (1992) The system H_2O-NaCl. PACROFI IV, program and abstracts. pp 108–111

Bozzo AT, Chen JR, Barduhn AJ (1973) The properties of hydrates of chlorine and carbon dioxide. In: Delyannis A, Delyannis E (eds) Fourth International Symposium on Fresh Water from the Sea 3:437–451

Burnard PG, Hu RZ, Turner G, Bi XW (1999) Mantle, crustal and atmospheric noble gases in Ailaoshan gold deposits, Yunnan Province, China. Geochim Cosmochim Acta 63:1595–1604

Cai HY, Zhang GL (1983) On submarine volcanism hot spring (exhalative) mineralization of the Dachang tin polymetallic deposit in Guangxi. Bull Inst Min Res Geol 1(4):13–21(in Chinese)

Cai MH, Liang T, Wu DC, Huang HM (2004) Structural feature and its control of mineralization of the Nandan-Hechi metallogenic belt in Guangxi Province. Geology and Exploration 6:5–10 (in Chinese with English abstract)

Cai MH, He LQ, Liu GQ, Wu DC, Huang HM (2006a) SHRIMP zircon U–Pb dating of the intrusive rocks in the Dachang tin polymetallic ore field, Guangxi and their geological significance. Sov Sci Rev Sect G Geol Rev 3:407–414 (in Chinese with English abstract)

Cai MH, Liang T, Wei KL, Huang HM, Liu GQ (2006b) Rb–Sr dating of the no.92 orebody of the Tongkeng-Changpo deposit in the Dachang tin polymetallic ore field, Guangxi, and its significance. Geology and Mineral Resources of South China 2:35–42 (in Chinese with English abstract)

Chappell BW, White AJR (1974) Two contrasting granite types. Pac Geol 8:173–174

Chen HD, Zeng YF, Li XQ (1989) Evolution of the sedimentation and tectonics of late Paleozoic Danchi basin. Acta Sedimentologica Sinica 7(4):85–96 (in Chinese with English abstract)

Chen YC, Huang MZ, Xu J, Hu YZ, Tang SH, Li YQ, Meng LK (1993) Tin deposits of Dachang. Geological Publishing House, Beijing, pp 53–311(in Chinese with English abstract)

Diamond LW (2001) Review of the systematics of CO_2-H_2O fluid inclusions. Lithos 55:69–99

Ding TP, Peng ZC, Li H, Li YH (1988) Stable isotope studies on several typical mineral deposits. Science and Technology Publishing House of Beijing, Beijing, pp 21–44 (in Chinese with English abstract)

Fu M, Changkakoti A, Krouse HR, Gray J, Kwak TAP (1991) An oxygen, hydrogen, sulfur, and carbon isotope study of carbonate-replacement (skarn) tin deposits of the Dachang tin field, China. Econ Geol 86:1683–1703

Fu M, Kwak TAP, Mernagh TP (1993) Fluid inclusion studies of zoning in the Dachang tin polymetallic ore field, People's Republic of China. Econ Geol 88:283–300

Giggenbach WF (1986) The use of gas geochemistry in delineating the origin of fluid discharges over the Taupo volcanic zone: a review. In: 5th International Volcanological Congress, Volcanism, Hydrothermal Systems, and Related Mineralization, Hamilton, Newland, February 1986. Proceedings, pp 47–50

Han F, Zhao RS, Shen JZ, Hutchinson RW, Jiang SY (1997) Geology and origin of ores in the Dachang polymetallic tin ore field. Geological Publishing House, Beijing, pp 65–157 (in Chinese with English abstract)

Hu RZ, Zhong H, Ye ZJ, Bi XW, Turner G, Burnard PG (1998) Helium and argon isotopic geochemistry of Jinding large-scale lead–zinc deposit. Sci China Ser D 28(3):208–213 (in Chinese)

Hu RZ, Bi XW, Turner G, Burnard PG (1999) Helium and argon isotopic geochemistry of gold mineralizing fluid of Ailaoshan gold mineralization belt. Sci China Ser D 29:321–330 (in Chinese)

Jean-Baptiste P, Fouquet Y (1996) Abundance and isotopic composition of helium in hydrothermal sulfides from the East Pacific Rise at 13°N. Geochim Cosmochim Acta 60:87–93

Lattanzi P, Corazza M, Corsini F, Tanelli G (1989) Sulfide mineralogy in the polymetallic cassiterite deposits of Dachang, P. R. China. Mineral Deposits 24:141–147

Lei LQ (1986) Preliminary discussion of genesis of the Dachang Changpo polymetallic tin deposit. Mineral Deposits 5:87–96 (in Chinese)

Li YQ, Chen WS (1989) The ore-forming fluid of Dachang tin deposit. Acta Petrologica Sinica (3):12–24 (in Chinese with English abstract)

Liu B, Shen K (1999) Thermodynamics of fluid inclusions. Geological Publishing House, Beijing, pp 44–118 (in Chinese with English abstract)

Pašava J, Kříbek B, Dobeš P (2003) Polymetallic tin sulfide deposits in the eastern part of the Dachang tin field (South China) and the role of black shales in their origin. Mineral Deposits 38:39–66

Qin DX, Hong T, Tian YL, Chen JW (2002) Ore geology and technical economy of no.92 orebody of the Dachang tin deposit, Guangxi. Geological Publishing House, Beijing, pp 31–132 (in Chinese with English abstract)

Roedder E (1984) Fluid inclusions. Rev Mineral 12:25–35

Rui ZY, Li YQ, Wang LS (2003) Approach to ore forming conditions of ore fluid inclusions. Mineral Deposits 22:13–23 (in Chinese with English abstract)

Simmons SF, Sawkins FJ, Schulutter DJ (1987) Mantle-derived heliumin: two Peruvian hydrothermal ore deposits. Nature 329:429–432

Stuart FM, Turner G, Duckworth RC, Fallick AE (1994) Helium isotopes as tracers of trapped hydrothermal fluids in ocean-floor sulfides. Geology 22:823–826

Stuart FM, Burnard P, Taylor RP, Turner (1995) Resolving mantle and crustal contributions to ancient hydrothermal fluids: He–Ar isotopes in fluid inclusions from Dae Hwa W-Mo mineralisation, South Korea. Geochim Cosmochim Acta 59:4663–4673

Tanelli G, Lattanzi P (1985) The cassiterite-polymetallic sulfide deposits of Dachang (Guangxi, People's Republic of China. Mineral Deposits 20:102–106

Wang DH, Chen YC, Chen W, Sang HQ, Li HQ, Lu YH, Chen KL, Lin ZM (2004) Dating of the Dachang superlarge tin polymetallic deposit in Guangxi and its implication for the genesis of the no. 100 orebody. Acta Geol Sinica (English edition) 78:452–458

Ye XS, Yan YX, He HZ (1999) The mineralization factors and tectonic evolution of Dachang superlarge tin deposit, Guangxi, China. Geochim 28:213–221 (in Chinese with English abstract)

Zhang GL, Cai HY (1987) Genesis of the Dachang Changpo polymetallic tin deposit. Geol Rev 33:426–436 (in Chinese)

Zhang WH, Chen ZY (1993) Geology of fluid inclusions. China University of Geosciences Press, Wuhan, pp 83–156 (in Chinese)

Zhao KD, Jiang SY, Xiao HQ, Ni P (2002) Origin of ore-forming fluids of the Dachang Sn-polymetallic ore deposit: evidence from helium isotopes. Chin Sci Bull 12:1041–1045 (English edition)